



Influence of Earthquake Parameters on the Bi-directional Behavior of Base Isolation Systems

Dana Abed ¹, Jafar Al Thawabteh ¹, Yazan Alzubi ^{1*}, Jamal Assbeihat ¹,
Eid Al-Sahawneh ¹

¹ Civil Engineering Department, Faculty of Engineering Technology, Al-Balqa Applied University, Amman, Jordan.

Received 15 July 2022; Revised 10 September 2022; Accepted 19 September 2022; Published 01 October 2022

Abstract

The introduction and development of the base isolation systems, especially the friction isolator device, were done recently to improve the capacity of adaptive behavior. The efficiency of multi-phase friction pendulums comes from their complexity, which helps reduce the structural responses and enhance structures' energy dissipation under lateral loads. Nevertheless, the influence of various earthquakes' properties on the behavior of base-isolation systems subjected to bi-directional seismic loading is still unclear. Hence, further research and studies regarding the behavior and capability of these systems under bi-directional loading are still necessary before incorporating this device in real-life practical applications. Therefore, this paper is intended to investigate the bi-directional behavior of the friction isolator subjected to various ground motion records. In order to do so, different versions of the friction pendulum system are selected and compared within the study context. Generally, the study's results have shown that the behavior of the friction isolator is highly dependent on low values of the PGA/PGV ratio. Besides, pulse-like earthquakes considerably impact the response of the isolator compared to non-pulse-like ones.

Keywords: Base Isolation System; Friction Pendulum; Lead Rubber; Bi-directional Behavior.

1. Introduction

One of the risk-mitigation strategies is implementing the seismic isolation system as a technique to improve the performance of structures subjected to seismic shaking intensity [1- 3]. The seismic isolation system has been utilized in seismic risk mitigation for decades. The first incorporation of this system in buildings occurred in San Francisco in 1870 [4- 6]. These systems showed good behavior and have been developed on a large scale for protecting various types of buildings against seismic events [7- 9]. The focus on the performance of these isolation systems subjected to pulse-like earthquakes has increased recently. The coupling of the bearing model subjected to bi-directional excitation is applied orthogonally through a circular yield surface [10]. In fact, a different number of generations of friction pendulum isolators have been introduced and developed in recent decades, such as double and triple friction pendulum isolators, where extensive investigation and reporting of the results regarding the performance of these isolation devices have been performed.

Hashemi & Aghashiri [11] investigated the seismic behavior of a rectangular base-isolated structure under bi-directional ground motion records. Rawat et al. [12] evaluated the performance of a cylindrical, base-isolated, steel liquid storage tank under bi-directional seismic loads. A similar investigation was conducted by Vern et al. [13]. Generally, the response of the base-isolation system varies greatly when considering the effects of bi-directional loading [14]. A similar conclusion was previously highlighted by Jing et al. [15].

* Corresponding author: yazan.alzubi@bau.edu.jo

 <http://dx.doi.org/10.28991/CEJ-2022-08-10-02>



© 2022 by the authors. Licensee C.E.J, Tehran, Iran. This article is an open access article distributed under the terms and conditions of the Creative Commons Attribution (CC-BY) license (<http://creativecommons.org/licenses/by/4.0/>).

It can be seen that considered bi-directional loading during the investigations of base-isolated structures is significantly important. Nevertheless, the literature is still missing a study investigating the effects of various earthquakes on the bi-directional performance of different base isolation systems. Therefore, the objective of this study is to evaluate the influence of peak ground acceleration on peak ground velocity ratio (PGA/PGV), distance to fault rupture, and pulse-like properties, as well as the effect of pulse period on the bi-directional behavior of different friction pendulum isolators. As a part of the study, the behavior of five friction isolation systems modeled with different friction surfaces under the effect of various ground motion records will be assessed and compared to the behavior of the lead rubber bearing isolator. In addition, the same values of effective damping ratio and period will be used for the different friction isolation systems. This study is devoted to filling the gap in the literature and providing a crucial evaluation of the behavior of these base isolation systems for practical applications in earthquake-prone countries.

2. Selected Isolation Systems

The first record of the implementation of a lead rubber bearing isolator (LRB) was in the late seventies in New Zealand [16]. The isolator comprises a lead core, various elastomeric bearing layers, rubber, and stiffening steel plates introduced alternatively [17]. Generally, the plastic deformation of the lead core in the LRB isolator causes a hysteretic dissipation of the energy [4]. Bouc-Wen or rate-independent plasticity model can be performed to analyze the shear force-horizontal deformation response of LRB [18]. The modeling of the LRB isolator governs the nonlinear force-deformation behavior depending on the characteristic strength (Q_d), elastic stiffness (K_e), post-elastic stiffness ($K_d = K_e/\alpha$), and yield displacement (D_y) as shown in Equation 1.

$$D_y = \frac{Q_d}{K_e - K_d} \quad (1)$$

The effective stiffness (K_{eff}) of LRB is the result of the secant slope to the design displacement of the isolator (D_{design}), as illustrated in Equation 2.

$$K_{eff} = K_d + \frac{Q_d}{D_{design}} \quad (2)$$

Zayas et al. [19] introduced friction pendulum (FP) as one of the most prevailing base isolation systems. It is composed of a spherical concave dish, which produces the restoring force and friction, generating hysteresis behavior [3]. The isolator practicality emerges from the operation of high displacements with small sizes, the elimination of any torsional influences on asymmetrical structures, and the isolation of the vibration period of the isolator from the weight of the superstructure [20]. The modeling of the FP isolator is controlled by the bi-linear hysteretic model based on the friction coefficient (μ), weight (W), and the radius of curvature of the sliding surface (R) in order to compute the effective stiffness (K_{eff}) of FP device using Equation 3.

$$K_{eff} = \frac{W}{R} + \frac{\mu W}{D_{design}} \quad (3)$$

A double friction pendulum (DFP) is a multi-staged isolator that consists of an internal hinged slider inserted between two opposite concave surfaces where the primary function of the slider is to modify the disparity caused by the rotations of the top and bottom parts of the hinged slider as a result of the imbalance friction generated by the two sliding surfaces. Furthermore, another function of the device is the uniform transfer of the load to the surface to avoid any likely excessive wear that could subsequently develop a significant variance regarding the friction properties of the isolator. The fundamental benefit of deploying DFP is the profitability in consequence of the small dimensions and the adjustability due to the selection of suitable hysteric characteristics at diverse bearing phases under various inputs of seismic excitation [21, 22]. The hysteresis behavior is characterized by Fenz and Constantinou [21] for determining the effective stiffness of the bearing, as illustrated in Equation 4.

$$K_{eff} = \frac{F_{f2} + \left(\frac{W}{R_{eff1} + R_{eff2}} \right) \times (D_{design} - u^*)}{D_{design}} \quad (4)$$

where F_{f2} is the lateral force in the isolator during the second operation stage, and R_{eff1} and R_{eff2} are the effective radii of the first and second surfaces, respectively.

Triple friction pendulum (TFP) is a multi-staged isolator that consists of a rigid internal slider inserted between four concave surfaces packed in series. This device includes three distinctive processes of the pendula as the result of the existence of two inner surfaces with identical properties. In fact, the mechanisms of double and triple friction pendulum isolators are demonstrated in the simultaneous restriction of the story acceleration and base displacement via the alternation of different combinations of stiffness and damping values over the entire range of motion of these devices [23, 24]. The main merit of this isolator is its adaptability in choosing desirable stiffness and damping combinations at various stages under various inputs of ground motion records providing accessibility of these devices in several levels

of performance objective in comparison to conventional base isolation systems [21, 25-27]. Based on that, the best base isolator in the performance-based design scenarios can debatably be the TFP isolator because of the ability to adequately select unique friction radius values and coefficient values at every stage of the isolator [28]. The hysteresis behavior of the TFP isolator is defined by Fenz & Constantinou [21], similar to the DFP isolator for calculating the effective stiffness of TFP, as shown in Equation 5.

$$K_{eff} = \frac{F_{f4} + \left(\frac{W}{R_{eff1} + R_{eff4}}\right) \times (D_{design} - u^{**})}{D_{design}} \tag{5}$$

where F_{f4} is the lateral force in the isolator during the fourth operation stage, and R_{eff1} and R_{eff4} are the effective radii of the first and fourth surfaces, respectively.

3. Materials and Methods

As mentioned previously, this study is intended to investigate the performance of various base-isolation systems subjected to earthquakes with different characteristics. The methodology that was adopted during the analysis is shown in Figure 1. Generally, the study analysis started by developing the finite element models and selecting the ground motion records. Thereafter, various base-isolation systems are designed, and the analysis is performed. Finally, the results are reported and discussed.

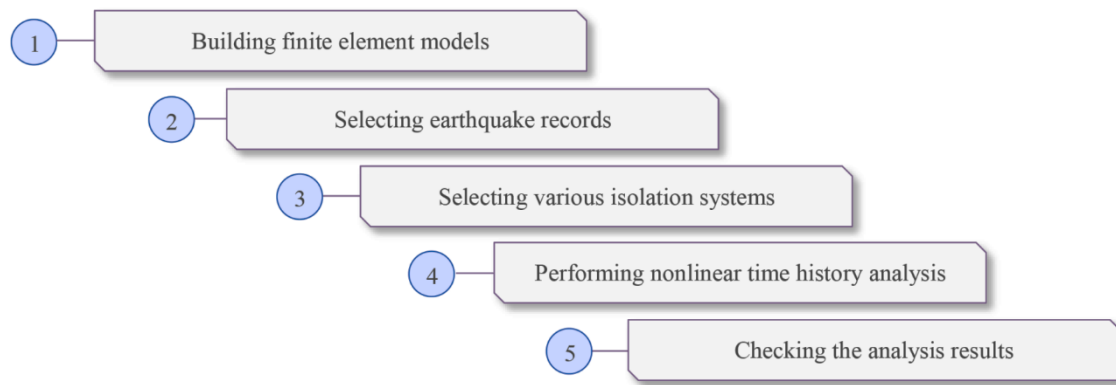


Figure 1. A summary of the research methodology adopted in this study

Two critical parameters of the isolator were maintained constant for all evaluated isolators to perform a restricted comparison between these systems. The effective period and damping parameters were computed using Equations 7 and 8, respectively.

$$T_{eff} = \sqrt{\frac{W}{K_{eff}g}} \tag{7}$$

$$\zeta_{eff} = \frac{\text{Area of the hysteresis loop}}{2\pi * K_{eff} * D_{design}^2} \tag{8}$$

where W is the total weight on the isolator, K_{eff} is its effective stiffness, D_{design} is the isolator's design capacity, and g is the gravitational acceleration.

Consequently, a trial and error procedure was conducted to meet the above-described requirement for determining the characteristics of friction pendulum bearings, as illustrated in Table 1, and the properties of the LRB isolator, as shown in Table 2. These isolators were all designed to achieve 3 seconds and a 15% damping ratio with an ultimate displacement of 0.57 m.

Table 1. Selected properties of the friction pendulum isolators

Isolator Type	FP	DFP		TFP			
Surface	-	1	2	1	2	3	4
R	3.1	1.6	1.8	1.7	0.62	0.62	1.7
μ	0.031	0.02	0.042	0.15	0.1	0.1	0.15
h	0.35	0.15	0.15	0.24	0.08	0.08	0.24
d	-	0.25	0.38	0.03	0.01	0.01	0.05

Table 2. Selected properties of the lead rubber bearing

k_d	670
Q_d	68
α	10

Within the scope of the paper, suitable ground motion records were carefully selected due to their remarkable impact on the results of this study. Hence, Pacific Earthquake Engineering Research Center (PEER) website was used to download many real earthquake records to pre-process the data and obtain adequate records for the analysis. In addition, the adoption of Baker's approach [29] based on wavelet decomposition was done during the pre-processing phase for classifying the components of each earthquake into pulse-like or non-pulse-like. Based on that, the calculation of the factors, including PGV, the pulse indicator (I_p) as shown in Equation 9, and the late arrival parameters present the time that corresponds to 20% energy of the total cumulative energy in the original signal ($t_{20\%,orig}$) as well as the 10% energy of the total cumulative energy in the extracted pulse signal ($t_{10\%,pulse}$) were performed. Thereafter, the criterion defined by Baker [29] was followed where the value of I_p is larger than 0.85, the value of PGV of the original ground motion is larger than 0.3 m/s, and $t_{20\%,orig}$ is larger than $t_{10\%,pulse}$.

$$I_p = \frac{1}{1 + e^{-23.3 + 14.6(\text{PGV ratio}) + 20.5(\text{energy ratio})}} \tag{9}$$

where I_p is the pulse indicator, the PGV ratio is the PGV of the residual signal divided by the PGV of the original signal, and the energy ratio is defined as the residual signal's energy divided by the original signal's energy.

In general, four different types of ground motions were selected in this study. The first category was utilized to evaluate the influence of fault distance solely. In addition, the first category includes four non-pulse-like records of the Chi-Chi earthquake with RSNs: 1288, 1504, 1541, and 1545. Indeed, the Chi-Chi earthquake that occurred on 21 September 1999 is considered a very catastrophic event with 2415 people killed, 11,305 injured, and over NT\$300 billion worth of damages. The selection of these earthquake records helps investigate the influence of the closest distance to the fault (R_{rup}). Hence, the value of other earthquake parameters such as PGA, PGA/PGV ratio, and shear-wave velocity (V_{s30}) was kept constant in order to eliminate their effects by applying these records as unscaled loads. The second category was obtained to assess the influence of pulse presence in the ground motion record, where it includes (RSNs 1504 and 1505) as the non-pulse-like and pulse-like earthquake records, respectively. Moreover, the value of earthquake parameters, including R_{rup} , PGA/PGV, and V_{s30} , were maintained to a very close range. Nonetheless, the value of PGA exhibited a significant disparity between these two ground motion records, as illustrated in Table 3, which necessitated rectifying this issue by scaling the earthquake records to the same target spectrum over the same range of periods. The third category was intended to highlight the influence of the pulse period (T_p) on the performance of the isolation systems, where this category includes three various earthquakes (RSNs: 185, 1505, and 4084). Accordingly, pulse periods were determined using wavelet decomposition and then were scaled to the same target spectrum as illustrated in Figure 2. The last category of ground motion was used to evaluate the impact of the PGA/PGV ratio where three records of the Parkfield-02 earthquake (RSNs: 4098, 4115, and 4126) were obtained, accounting for each group of PGA/PGV ratios in accordance with Zhu et al. [30]. The low class represents the first group of PGA/PGV ratios which is smaller than 0.8, while the second class is medium which ranges between 0.8 and 1.2, and the last class is high, which includes values greater than 1.2. The other earthquake parameters, such as R_{rup} , V_{s30} , and T_p , demonstrated close values except for PGA, where scaling the ground motion records was conducted to solve the issue.

Table 3. Selected earthquake records for NRHA

Earthquake Name	Magnitude	R_{rup} (km)	V_{s30} (m/s)	Direction	T_p (s)	I_p	PGA	PGV	PGA/PGV
Imperial Valley-06	6.53	7.5	202.89	X	5.145	1.000	0.258	0.532	0.486
				Y	3.766	1.000	0.221	0.515	0.430
Chi-Chi	7.62	45.89	459.67	X	-	-	0.083	0.112	0.742
				Y	-	-	0.076	0.137	0.553
Chi-Chi	7.62	0.62	433.63	X	-	-	0.499	0.921	0.542
				Y	-	-	0.319	0.513	0.622
Chi-Chi	7.62	0.32	487.34	X	13.307	1.000	0.512	2.496	0.205
				Y	11.949	1.000	0.371	2.641	0.140
Chi-Chi	7.62	12.38	493.09	X	-	-	0.189	0.421	0.449
				Y	-	-	0.136	0.523	0.259
Chi-Chi	7.62	7.4	459.34	X	-	-	0.228	0.598	0.380
				Y	-	-	0.197	0.347	0.569
Parkfield-02	6	2.68	269.55	X	1.197	0.998	0.238	0.332	0.717
				Y	1.309	1.000	0.290	0.474	0.611

Parkfield-02	6	3	326.64	X	1.302	1.000	0.440	0.402	1.096
				Y	0.868	1.000	0.361	0.393	0.919
Parkfield-02	6	2.65	265.21	X	1.197	1.000	0.276	0.399	0.693
				Y	1.379	1.000	0.307	0.469	0.654
Parkfield-02	6	3.79	260.63	X	0.637	1.000	0.683	0.360	1.896
				Y	0.567	0.992	0.833	0.399	2.089

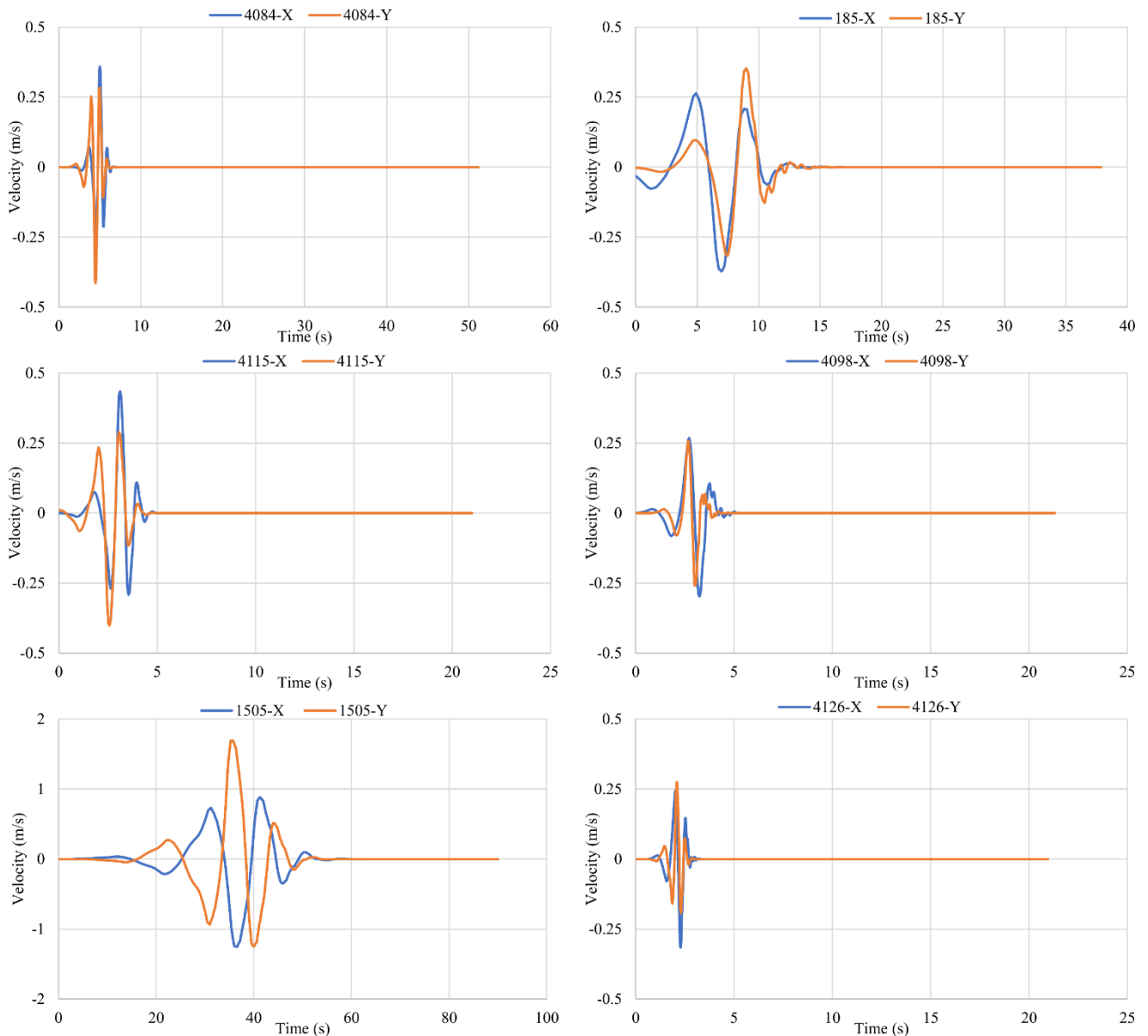


Figure 2. Extracted pulse signal for both directions of the earthquakes

Various methods of scaling earthquake records, such as ASCE [31], ACT [32], and the mean square error (MSE), were investigated by Michaud and Léger [33], where it was concluded that the MSE approach reflected the best accuracy in contrast to the other scaling approaches and hence was selected for conducting this study. Scaling the ground motion records using the MSE approach requires selecting a single scaling factor to reduce the MSE between the record and the target spectrums for achieving the best match of these spectrums over an adequate period. Generally, scaling earthquake records for isolated buildings using the ASCE 41-17 code demands scaling over the periods between $0.75 T_x$, calculated using upper-bound isolator characteristics, and $1.25 T_x$, calculated using lower-bound isolator characteristics. This criterion was used for scaling all earthquakes except for the closest distance to the rupture surface, where the records were used as undisturbed not to impact the change in PGA value over the distance.

4. Results and Discussions

As discussed earlier, the first category of ground motion records, which includes four records of the Chi-Chi earthquake, was obtained to study the influence of the closest distance to the rupture plane on the behavior of several isolators in terms of the peak base shear, displacement, and dissipated energy responses. Accordingly, a thorough selection of the earthquake records was conducted to neutralize the potential biases in the results that arise from any disparities. As can be observed in Figure 3, the same pattern was expressed by all evaluated base isolation systems subjected to all rupture distances where the rupture distance exhibited an inversely proportional relationship with the base shear response where any increase in the rupture distance resulted in a decrease in the base shear results. In addition, the TFP isolator showed the highest base shear values compared to other base isolation devices, where the highest result was seen at approximately 2000 kN. On the other hand, all the investigated isolators reflected the same performance as the rupture distance increased, where similar base shear results were achieved at the last value in the trend. However, the lowest base shear response was recorded in the case of the FP isolator, where the lowest base shear value was observed at 390 kN. Regarding the peak displacement response, the same trend was exhibited by all investigated base isolation systems where the displacement response reflected the highest values at the lowest rupture distance and constantly reduced with the increase in the rupture distance. All assessed isolators demonstrated similar displacement values at the start and end of the trend, and the LRB isolator expressed the highest displacement value at 0.5 m, while the FP isolator exhibited the lowest value at 0.02 m. The same conclusion can be drawn for the dissipated energy, where the reduction in the response is associated with the increase in the closest distance to the rupture plane for all isolators.

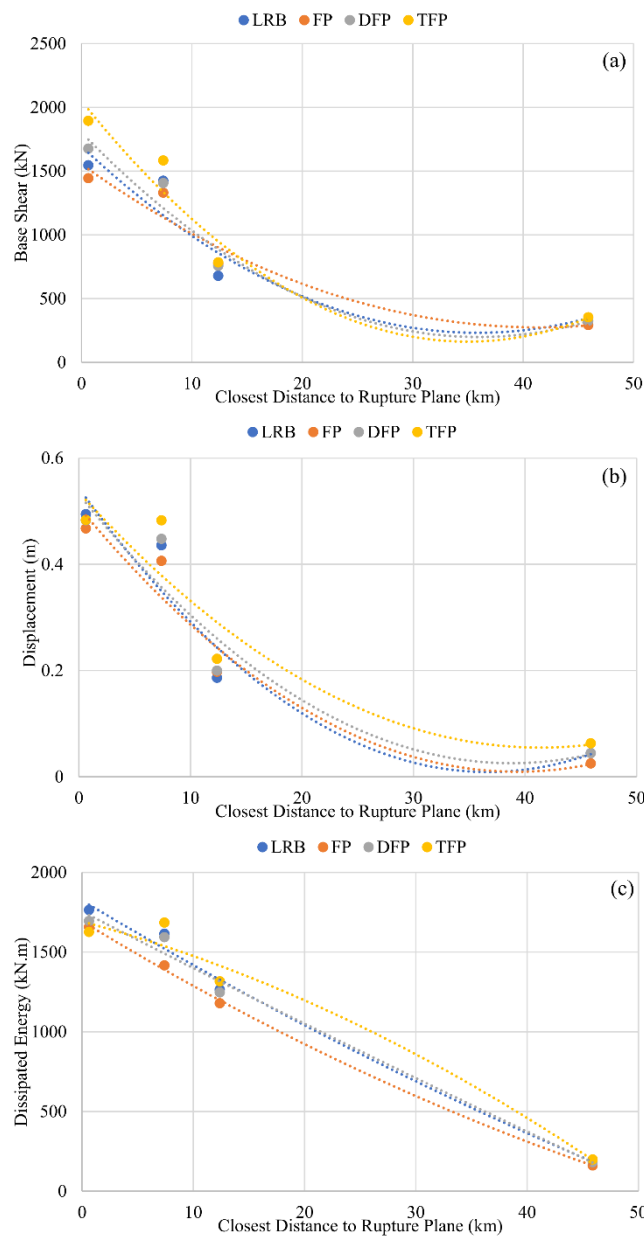


Figure 3. Influence of the closest distance to the rupture plane on the peak response of each isolation system (a) base shear; (b) isolator displacement; (c) dissipated hysteretic energy

The highest and lowest dissipated energy values were seen close for all base isolation systems. Nonetheless, the LRB isolator marked the highest dissipated energy result roughly at 1800 kN.m, and the FP isolator achieved the lowest dissipated energy value at 170 kN.m. The consistent trend of the increase in the responses accompanied by the decrease in the closest distance to the rupture plane can be explained due to poor performance in settling the base isolation system under the influence of near-fault earthquakes with respect to far-fault ones, which is caused by considerable destabilizing of the isolator [34].

As can be concluded from Figure 4, the displacement in the X direction for the two cases of closest distance to the rupture plane, which are 0.62 km and 7.4 km, surpassed the design displacement. In addition, the hysteresis behavior is inversely proportional to the Rrup, where any increase in the hysteresis behavior leads to a minimization in the Rrup value. Accordingly, the case of 0.62 km exhibited the largest hysteresis behavior compared to other cases, whereas the lowest hysteresis behavior was recorded for the case of 45.59 km.

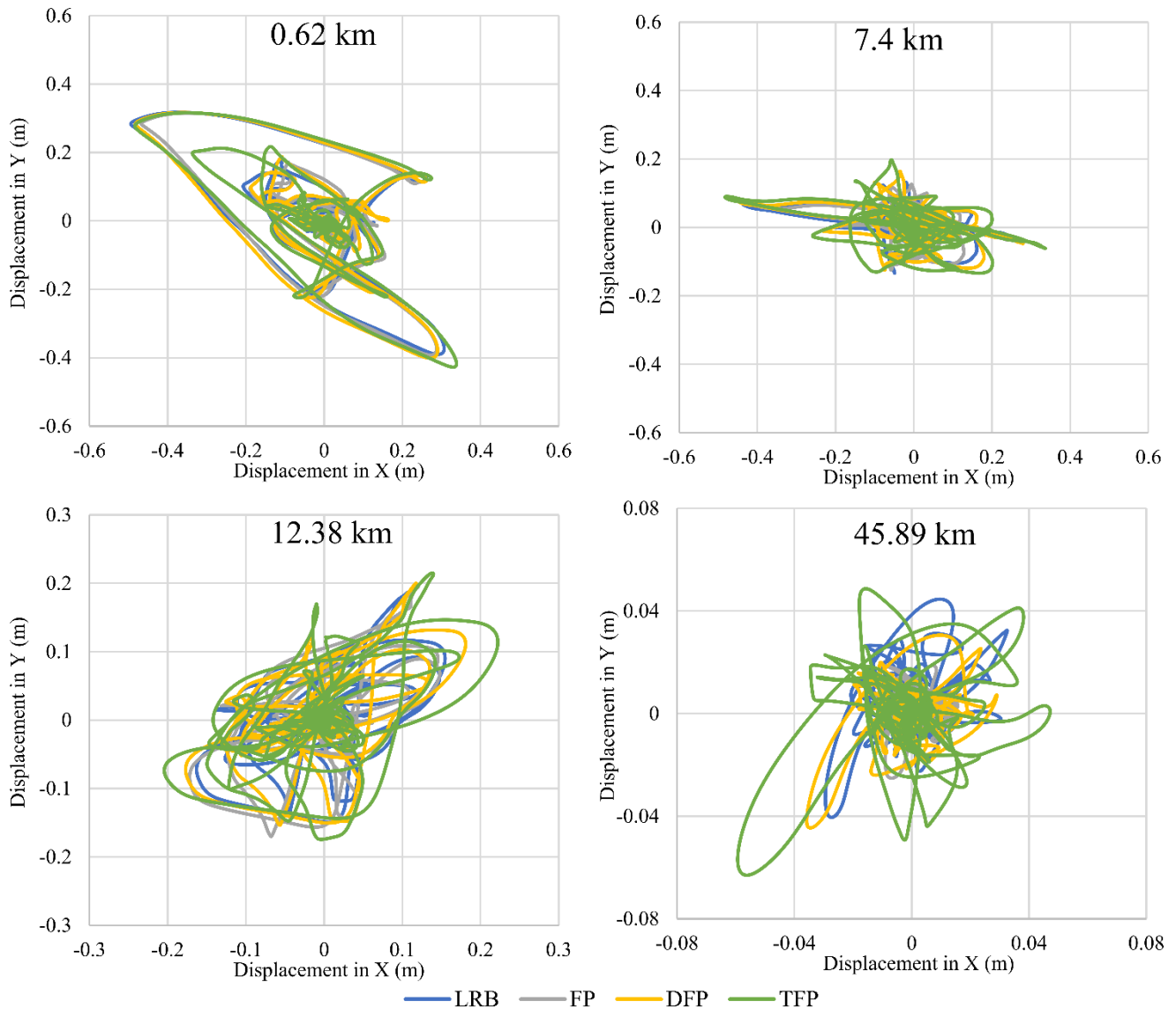


Figure 4. The hysteresis behavior of the investigated base isolation systems for the closest distance to the rupture plane

The second investigated category of earthquake records includes one ground motion record for each pulse-like and non-pulse-like case. This category is devoted to studying the efficiency of the base isolation systems in terms of the same three responses under the effect of pulse-like and non-pulse-like earthquakes. All examined isolators observed the same behavior for the base shear response, where pulse-like earthquakes reflected the highest base shear results compared to non-pulse-like earthquakes, as illustrated in Figure 5. The highest base shear response was viewed in the case of the DFP isolation system under pulse-like earthquake, where the highest result was seen roughly at 3100 kN. Moreover, LRB and FP isolators exhibited the same behavior subjected to pulse-like earthquakes where both marked the lowest base shear results, approximately 1500 kN. On the contrary, non-pulse-like earthquakes showed similar base shear results for all studied isolators. However, the FP isolator under a non-pulse-like earthquake recorded the lowest

base shear value at nearly 940 kN. In fact, all assessed base isolation systems expressed the same pattern for the peak displacement response, where pulse-like earthquakes displayed the highest displacement results in contrast to the non-pulse-like earthquake. However, very similar displacement values were achieved by all investigated isolators subjected to both pulse-like and non-pulse-like earthquakes. The highest displacement value was observed in the FP isolator at 0.51 m, while the lowest displacement result was marked at 0.25 m for the same isolation system. The final considered response is the dissipated energy, where the highest results were expressed for all examined base isolation systems under pulse-like earthquakes regarding the non-pulse-like earthquake. Pulse-like earthquakes marked similar dissipated energy results for LRB, DFP, and TFP isolators, where the highest value was reflected at 1200 kN.m, whereas the FP isolator displayed the lowest dissipated energy response roughly at 1100 kN.m. In the case of non-pulse-like earthquakes, the LRB base isolation system illustrated the highest dissipated energy value, particularly at 760 kN.m, while the lowest result was recorded at 690 kN.m in the case of FP and TFP isolators. Based on the results, the efficacy of all base isolation systems was compromised under the influence of pulse-like earthquakes, which can be attributed to the great seismic demands due to the high energy and low-frequency characteristics of this earthquake compared to non-pulse-like earthquakes [35].

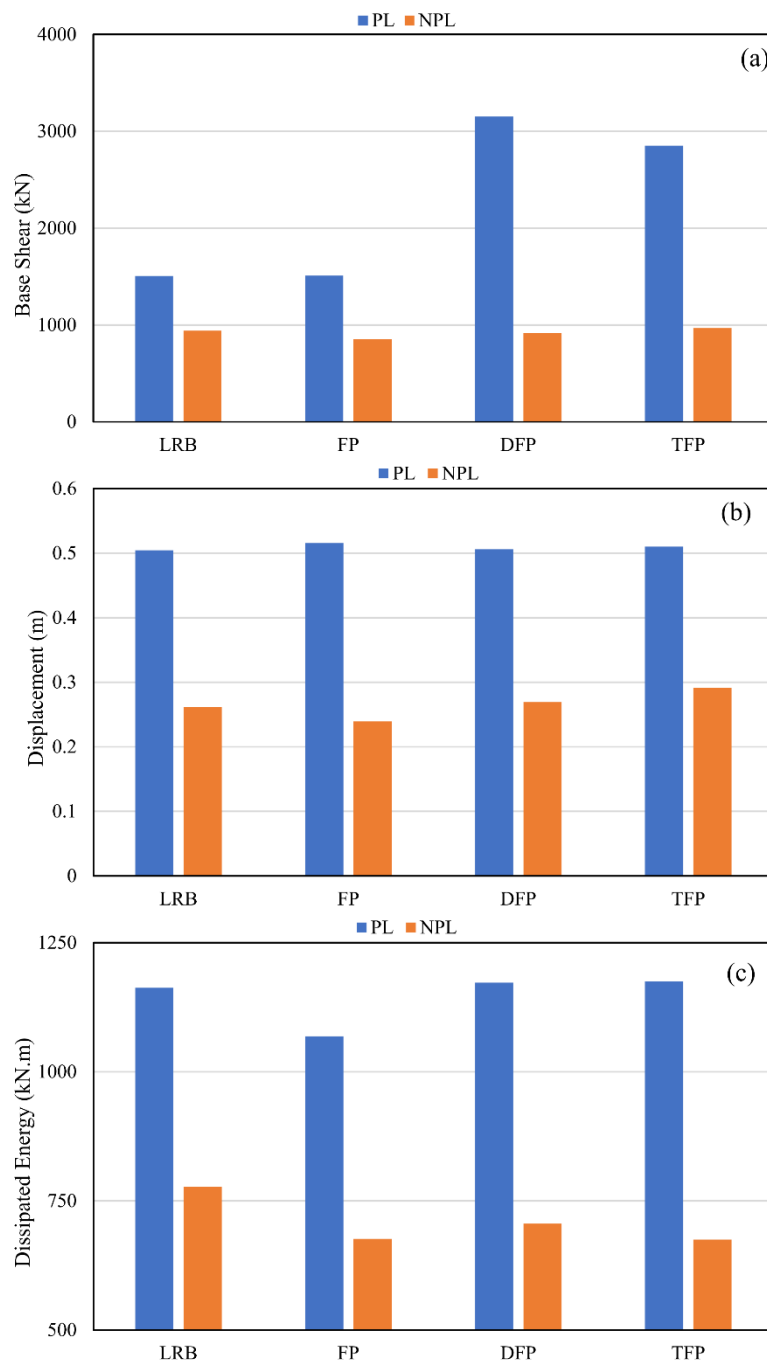


Figure 5. Effect of the pulse-like earthquake on the peak response of each isolation system (a) base shear; (b) isolator displacement; (c) dissipated hysteretic energy

The hysteresis behavior for pulse-like earthquakes exceeded the design displacement in the X direction, whereas the non-pulse-like earthquake displayed results within the limits of design displacement for both directions, as shown in Figure 6.

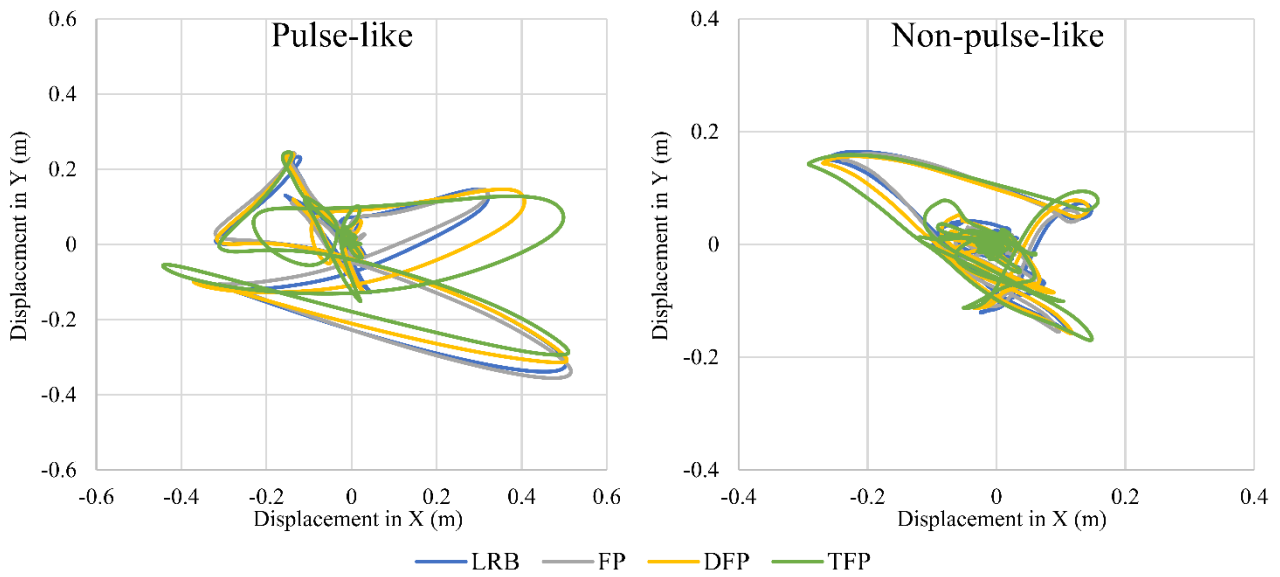
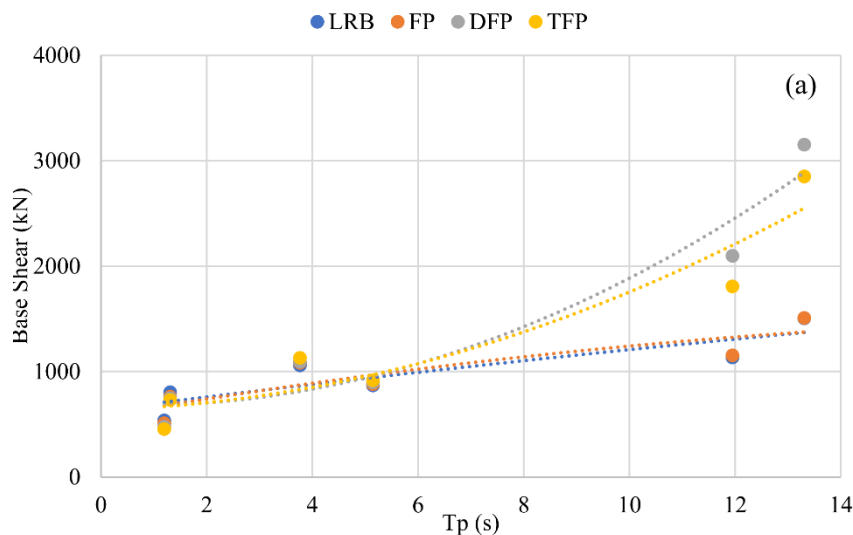


Figure 6. The hysteresis behavior of the investigated base isolation systems for pulse-like and non-pulse-like earthquakes

Three different earthquake records were selected to investigate the effect of the pulse period on the efficiency of various base isolation systems in terms of base shear, displacement, and dissipated energy responses. In general, all evaluated base isolation systems under the pulse period reflected the same trend for the base shear response, where the increase in the pulse period corresponds to the increase in the base shear results, as illustrated in Figure 7. The highest base shear value was expressed nearly at 3100 kN in the case of the DFP isolator. Additionally, all base isolation systems exhibited similar base shear values at the beginning point of the pattern. Nonetheless, the lowest base shear result was recorded at approximately 550 kN in the case of the TFP isolator. Regarding the peak displacement response, all examined isolators displayed an identical pattern where the increase in the pulse period increased the displacement results. The displacement response was observed to have comparable values at the start and end of the trend. However, the FP isolator demonstrated the highest displacement result marking 0.51 m, while the lowest displacement value was recorded at 0.1 m for the same base isolation system. The dissipated energy response exhibited the same pattern for all investigated isolators, where an increased pulse period led to increased dissipated energy results. TFP base isolation system reflected the highest and lowest dissipated energy results at 1250 and 350 kN.m, respectively. The analysis results have illustrated the impact of the pulse period on the performance of all base isolation systems where the pulse period is related to the increase in the responses. It can be attributed to the abnormal and remarkable seismic demands caused by the long-period pulses produced, particularly near-fault pulse-like earthquakes, irrespective of the base isolation system [36, 37].



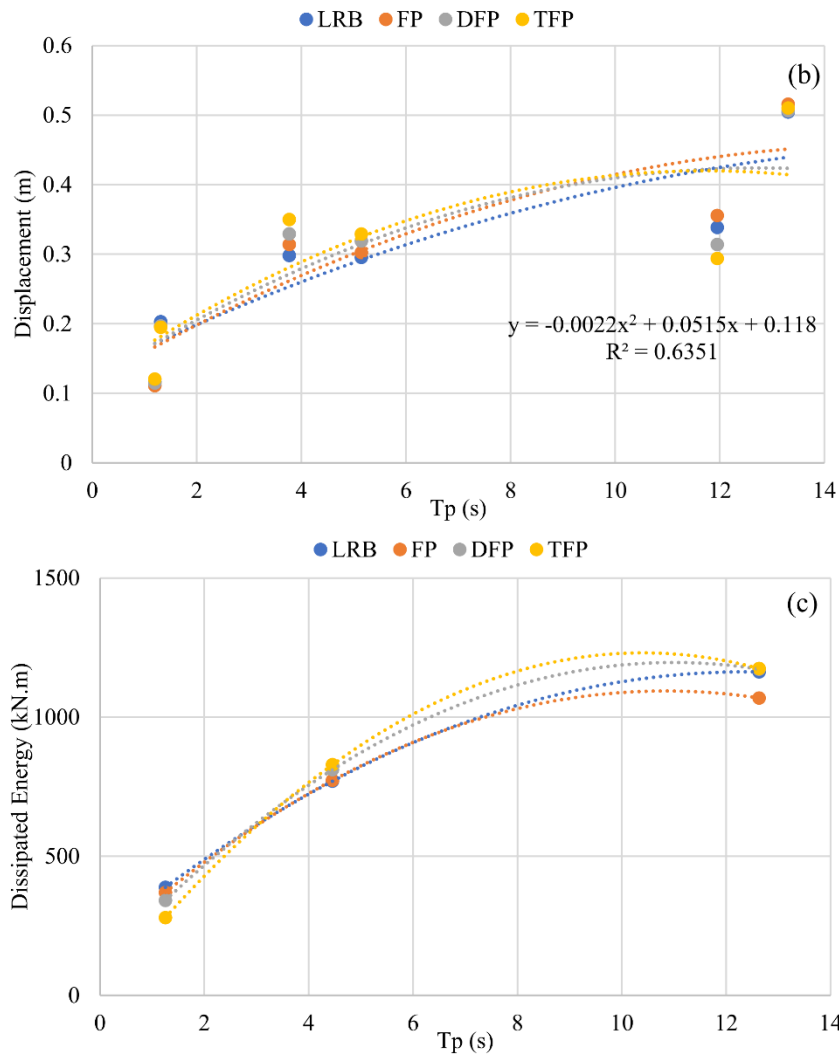
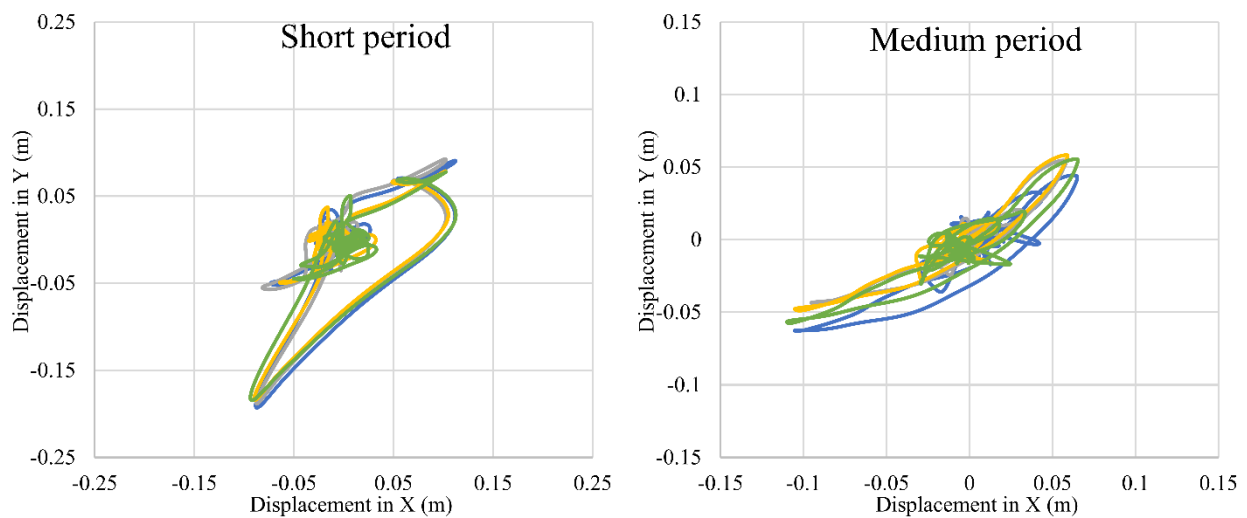


Figure 7. Effect of pulse period on the peak response of each isolation system(a) base shear; (b) isolator displacement; (c) dissipated hysteretic energy

As can be seen in Figure 8, the results of the three types of pulse period did not surpass the design displacement boundaries for both directions. Moreover, the largest hysteresis behavior was expressed by a short period followed by a medium and an extended period.



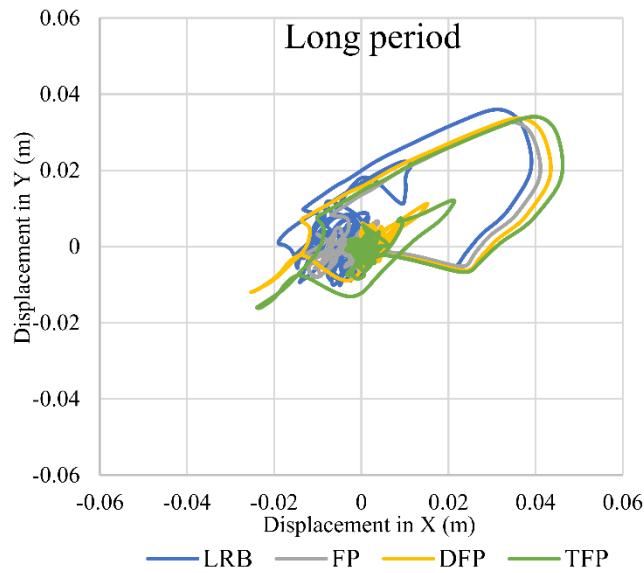


Figure 8. The hysteresis behavior of the investigated base isolation systems for the pulse period

The last category includes three records of the Parkfield-02 earthquake, which were utilized to assess the impact of the PGA/PGV ratio on the efficacy of different base isolation systems. As illustrated in Figure 9, the low PGA/PGV ratio showed the highest base shear results for all investigated base isolation systems compared to medium and high ratios.

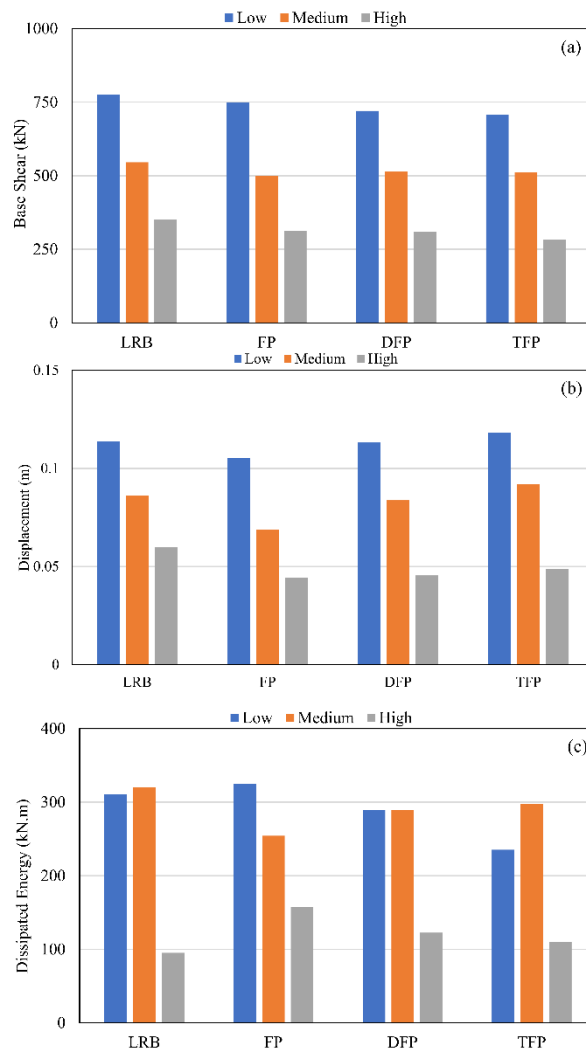


Figure 9. Effect of PGA/PGV ratio on the peak response of each isolation system (a) base shear; (b) isolator displacement; (c) dissipated hysteretic energy

The same behavior was observed for all isolators with similar base shear values. However, in contrast to other base isolation systems, the LRB isolator exhibited the highest base shear values for low, medium, and high PGA/PGV ratios. Furthermore, the highest base shear values expressed by the LRB isolator were seen at 760 kN, 530 kN, and 360 kN for the low, medium, and high PGA/PGV ratios, respectively. On the other hand, the TFP isolator displayed the lowest base shear response for low and high PGA/PGV ratios compared to other base isolation systems, whereas the FP isolator experienced the lowest base shear value for the medium PGA/PGV ratio. Accordingly, the TFP isolator demonstrated the lowest base shear results roughly at 735 kN and 280 kN for low and high PGA/PGV ratios, respectively, while the lowest base shear value for a medium PGA/PGV ratio was observed in the case of the FP isolator exactly at 500 kN. Regarding the peak displacement response, the LRB isolator exhibited the highest displacement result for a low PGA/PGV ratio compared to other isolators, particularly at 0.19 m. In contrast, the highest displacement response for medium and high PGA/PGV ratios was seen in the case of the TFP isolator at nearly 0.11 m and 0.049 m, respectively. The lowest displacement value for low PGA/PGV ratio was experienced in the cases of DFP and TFP isolators, roughly at 0.165 m, while for medium PGA/PGV ratio, the lowest displacement response was shown in the case of the FP isolator at 0.09 m, and the lowest displacement result for high PGA/PGV ratio was reflected at 0.04 m. The last investigated response is the dissipated energy, where the highest response for low and high PGA/PGV ratios was reflected in the FP base isolation system. On the contrary, the highest dissipated energy result for a medium PGA/PGV ratio was observed in the case of the LRB isolator. The highest dissipated energy result for low and high PGA/PGV ratios was shown at 330 kN.m and 160 kN.m, respectively, while the highest energy value for a medium PGA/PGV ratio was exhibited at nearly 320 kN.m in the case of the LRB base isolation system. On the contrary, the lowest dissipated energy value for low PGA/PGV ratio was recorded in the case of TFP isolator at approximately 240 kN.m, whereas the lowest energy result for medium PGA/PGV ratio was expressed in the case of FP isolator roughly at 270 kN.m and the lowest energy response for high PGA/PGV ratio was seen in the case of LRB isolator at 96 kN.m. Based on the results, flexible buildings were notably influenced by the low PGA/PGV ratio value since these buildings include significant periods, while high PGA/PGV ratio values critically affect stiff buildings with short periods [38].

Medium and high PGA/PGV ratios exhibited displacement values that exceeded the design displacement limit in both directions, as shown in Figure 10. The largest hysteresis behavior was experienced in the medium PGA/PGV ratio, followed by a high PGA/PGV ratio, and finally, a low PGA/PGV ratio.

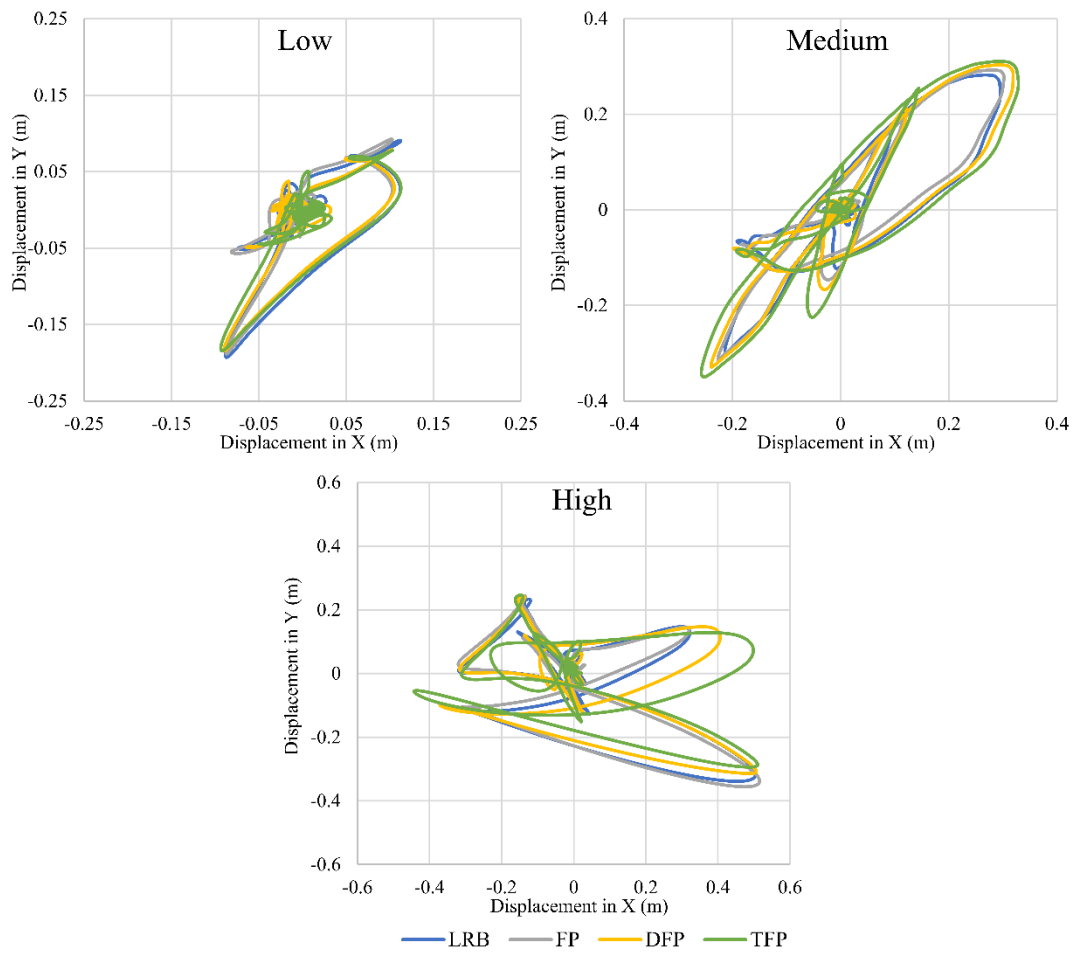


Figure 10. The hysteresis behavior of the investigated base isolation systems for the PGA/PGV ratio

5. Conclusions

This paper evaluated the bi-directional behavior of various base isolation systems subjected to controlled cyclic loads and seismic excitations. In addition, four groups of ground motion records were selected to investigate the effect of earthquake parameters, including the closest distance to the rupture plane, pulse existence, pulse period, and PGA/PGV ratio, on the efficiency and performance of different isolators. Based on the above statements, the following conclusions are made:

- TFP isolators expressed the highest peak base shear, displacement, and dissipated energy responses regarding the closest distance to the rupture plane parameter, where the increase in the rupture distance decreased all responses;
- Pulse-like earthquakes exhibited severe damage to all base isolation systems where the hysteresis behavior of pulse-like earthquakes exceeded the design displacement compared to the non-pulse-like earthquake;
- The pulse period parameter reflected a directly proportional relationship with the peak base shear, displacement, and dissipated energy responses, where the increase in the pulse period led to an increase in these responses;
- The highest results were shown in the low PGA/PGV ratio for all responses, followed by medium and high. This is because the low PGA/PGV ratio highly impacts flexible structures over long periods, in contrast to the high PGA/PGV ratio, which affects stiff structures over short periods.

6. Declarations

6.1. Author Contributions

Conceptualization, D.A., J.T., and Y.A.; methodology, D.A. and J.T.; formal analysis, D.A., J.T., Y.A., J.A., and E.A.; writing—original draft preparation, D.A., J.T., and Y.A.; writing—review and editing, J.A. and E.A.; visualization, Y.A., J.A., and E.A. All authors have read and agreed to the published version of the manuscript.

6.2. Data Availability Statement

The data presented in this study are available on request from the corresponding author.

6.3. Funding

The authors received no financial support for the research, authorship, and/or publication of this article.

6.4. Conflicts of Interest

The authors declare no conflict of interest.

7. References

- [1] Seo, C. Y., Karavasilis, T. L., Ricles, J. M., & Sause, R. (2014). Seismic performance and probabilistic collapse resistance assessment of steel moment resisting frames with fluid viscous dampers. *Earthquake Engineering and Structural Dynamics*, 43(14), 2135–2154. doi:10.1002/eqe.2440.
- [2] Kitayama, S., & Constantinou, M. C. (2018). Seismic Performance of Buildings with Viscous Damping Systems Designed by the Procedures of ASCE/SEI 7-16. *Journal of Structural Engineering*, 144(6), 4018050. doi:10.1061/(asce)st.1943-541x.0002048.
- [3] Becker, T. C., & Mahin, S. A. (2012). Experimental and analytical study of the bi-directional behavior of the triple friction pendulum isolator. *Earthquake Engineering and Structural Dynamics*, 41(3), 355–373. doi:10.1002/eqe.1133.
- [4] Warn, G. P., & Ryan, K. L. (2012). A review of seismic isolation for buildings: Historical development and research needs. *Buildings*, 2(3), 300–325. doi:10.3390/buildings2030300.
- [5] Touaillon, J. (1870). Improvement in buildings. US Letters Patent, (99973), United States of Patent and Trademark, Alexandria, United States.
- [6] Constantinou, M. C., Whittaker, A. S., Kalpakidis, Y., Fenz, D. M., & Warn, G. P. (2007). Performance of seismic isolation hardware under service and seismic loading. Technical Rep. No. MCEER-07, State University of New York, New York, United States.
- [7] Symans, M. D., Cofer, W. F., & Fridley, K. J. (2002). Base isolation and supplemental damping systems for seismic protection of wood structures: Literature review. *Earthquake Spectra*, 18(3), 549–572. doi:10.1193/1.1503342.
- [8] Robinson, W. H. (1982). Lead-rubber hysteretic bearings suitable for protecting structures during earthquakes. *Earthquake Engineering & Structural Dynamics*, 10(4), 593–604. doi:10.1002/eqe.4290100408.
- [9] Sasaki, T., Sato, E., Ryan, K. L., Okazaki, T., Mahin, S. A., & Kajiwara, K. (2012). NEES/E-defense base-isolation tests: effectiveness of friction pendulum and lead-rubber bearing systems. Proceedings of the 15th World Conference of Earthquake Engineering, 24-28 September, 2012, Lisbon, Portugal.

- [10] Abdel Raheem, S. E., & Hayashikawa, T. (2007). Bi-directional Seismic Response Control for Bridge Structures. IABSE Reports. doi:10.2749/weimar.2007.0068.
- [11] Hashemi, S., & Aghashiri, M. H. (2017). Seismic responses of base-isolated flexible rectangular fluid containers under horizontal ground motion. *Soil Dynamics and Earthquake Engineering*, 100, 159–168. doi:10.1016/j.soildyn.2017.05.010.
- [12] Rawat, A., Matsagar, V. A., & Nagpal, A. K. (2019). Numerical study of base-isolated cylindrical liquid storage tanks using coupled acoustic-structural approach. *Soil Dynamics and Earthquake Engineering*, 119, 196–219. doi:10.1016/j.soildyn.2019.01.005.
- [13] Vern, S., Shrimali, M. K., Bharti, S. D., Datta, T. K., & Noroozinejad Farsangi, E. (2022). Seismic Control of Base-Isolated Liquid Storage Tanks Subjected to Bi-directional Strong Ground Motions. *Arabian Journal for Science and Engineering*, 47(4), 4511–4530. doi:10.1007/s13369-021-06171-9.
- [14] Zelleke, D. H., Saha, S. K., & Matsagar, V. A. (2020). Multihazard Response Control of Base-Isolated Buildings under Bidirectional Dynamic Excitation. *Shock and Vibration*, 2020, 1-24. doi:10.1155/2020/8830460.
- [15] Jing, W., Cheng, X., & Shi, W. (2018). Dynamic Responses of Sliding Isolation Concrete Rectangular Liquid Storage Structure with Limiting Devices Under Bidirectional Earthquake Actions. *Arabian Journal for Science and Engineering*, 43(4), 1911–1924. doi:10.1007/s13369-017-2814-6.
- [16] Robinson, W. H., & Tucker, A. G. (1977). A lead-rubber shear damper. *Bulletin of the New Zealand Society for Earthquake Engineering*, 10(3), 151–153. doi:10.5459/bnzsee.10.3.151-153.
- [17] Kalpakidis, I. (2015). Lead-Rubber Bearings with Emphasis on Their Implementation to Structural Design. *Encyclopedia of Earthquake Engineering*, 1286–1295. doi:10.1007/978-3-642-35344-4_307.
- [18] Nagarajaiah, S., Reinhorn, A. M., & Constantinou, M. C. (1991). Nonlinear dynamic analysis of 3-D-base-isolated structures. *Journal of Structural Engineering*, 117(7), 2035-2054. doi:10.1061/(ASCE)0733-9445(1991)117:7(2035).
- [19] Zayas, V. A., & Mahin, S. A. (1987). The FPS earthquake resisting system experimental report. Report No. UCB/EERC87/01, Earthquake Engineering Research Center, University of California, Berkeley, United States.
- [20] Keikha, H., & Ghodrati Amiri, G. (2021). Seismic Performance Assessment of Quintuple Friction Pendulum Isolator with a Focus on Frictional Behavior Impressionability from Velocity and Temperature. *Journal of Earthquake Engineering*, 25(7), 1256–1286. doi:10.1080/13632469.2019.1568929.
- [21] Fenz, D. M., & Constantinou, M. C. (2008). Mechanical behavior of multi-spherical sliding bearings (No. 7). Technical Report MCEER-08-0007, State University of New York, New York, United States.
- [22] Fenz, D. M., & Constantinou, M. C. (2006). Behaviour of the double concave Friction Pendulum bearing. *Earthquake Engineering and Structural Dynamics*, 35(11), 1403–1424. doi:10.1002/eqe.589.
- [23] Tsai, C. S., Chen, B. J., Pong, W. S., & Chiang, T. C. (2004). Interactive behavior of structures with multiple friction pendulum isolation system and unbounded foundations. *Advances in Structural Engineering*, 7(6), 539–550. doi:10.1260/1369433042863189.
- [24] Moeindarbari, H., & Taghikhany, T. (2014). Seismic optimum design of triple friction pendulum bearing subjected to near-fault pulse-like ground motions. *Structural and Multidisciplinary Optimization*, 50(4), 701–716. doi:10.1007/s00158-014-1079-x.
- [25] Fenz, D. M., & Constantinou, M. C. (2008). Modeling triple friction pendulum bearings for response-history analysis. *Earthquake Spectra*, 24(4), 1011–1028. doi:10.1193/1.2982531.
- [26] Fenz, D. M., & Constantinou, M. C. (2008). Spherical sliding isolation bearings with adaptive behavior: Experimental verification. *Earthquake Engineering and Structural Dynamics*, 37(2), 185–205. doi:10.1002/eqe.750.
- [27] Malekzadeh, M., & Taghikhany, T. (2012). Multi-stage performance of seismically isolated bridge using triple pendulum bearings. *Advances in Structural Engineering*, 15(7), 1181–1196. doi:10.1260/1369-4332.15.7.1181.
- [28] Morgan, T. A., & Mahin, S. A. (2010). Achieving reliable seismic performance enhancement using multi-stage friction pendulum isolators. *Earthquake Engineering and Structural Dynamics*, 39(13), 1443–1461. doi:10.1002/eqe.1043.
- [29] Baker, J. W. (2007). Quantitative classification of near-fault ground motions using wavelet analysis. *Bulletin of the Seismological Society of America*, 97(5), 1486–1501. doi:10.1785/0120060255.
- [30] Zhu, T. J., Tso, W. K., & Heidebrecht, A. C. (1988). Effect of Peak Ground a/v Ratio on Structural Damage. *Journal of Structural Engineering*, 114(5), 1019–1037. doi:10.1061/(asce)0733-9445(1988)114:5(1019).
- [31] ASCE/SEI 7-10. (2013). Minimum design loads for buildings and other structures. American Society of Civil Engineers, Reston, United States. doi:10.1061/9780784412916.
- [32] Applied Technology Council. (2009). Quantification of building seismic performance factors. US Department of Homeland Security, FEMA, Washington, United States.

- [33] Michaud, D., & Léger, P. (2014). Ground motions selection and scaling for nonlinear dynamic analysis of structures located in Eastern North America. *Canadian Journal of Civil Engineering*, 41(3), 232–244. doi:10.1139/cjce-2012-0339.
- [34] Mazza, F., & Labernarda, R. (2018). Effects of nonlinear modelling of the base-isolation system on the seismic analysis of r.c. buildings. *Procedia Structural Integrity*, 11, 226–233. doi:10.1016/j.prostr.2018.11.030.
- [35] Chen, Z. Y., & Liu, Z. Q. (2019). Effects of pulse-like earthquake motions on a typical subway station structure obtained in shaking-table tests. *Engineering Structures*, 198, 109557. doi:10.1016/j.engstruct.2019.109557.
- [36] Pant, D. R., & Wijeyewickrema, A. C. (2013). Influence of near-fault ground motions on the response of base-isolated reinforced concrete buildings considering seismic pounding. *Advances in Structural Engineering*, 16(12), 1973–1988. doi:10.1260/1369-4332.16.12.1973.
- [37] Rostami, A., & Poursha, M. (2021). A lateral load distribution for the static analysis of base-isolated building frames under the effect of far-fault and near-fault ground motions. *Structures*, 34, 2384–2405. doi:10.1016/j.istruc.2021.08.125.
- [38] Elnashai, A. S., & Di Sarno, L. (2015). *Fundamentals of earthquake engineering: from source to fragility*. John Wiley & Sons, Hoboken, United States.